# Diffusive motions in liquid 18-crown-6: A molecular dynamics study

W. J. Briels and F. T. H. Leuwerink
*Chemical Physics Laboratory, University of Twente, P.O. Box 217, 7500 AE Enschede, The Netherlands*

(Received 13 February 1996; accepted 11 February 1997)

Transport properties of 18-crown-6 in the liquid phase are investigated by means of molecular dynamics simulations. Three different force fields are used. It is attempted to separate molecular motions into independent contributions from translations, rotations, and deformations. Translational diffusion coefficients are calculated and they are found to depend very much on the molecular flexibility, i.e., on the potential model. With two potential models, diffusion coefficients are obtained which are in good agreement with experimental data. With one of these force fields the possibility is investigated to define molecule-fixed frames which allow a separation of rotations and deformations. Two different definitions are suggested for this purpose. Combining contributions to the hydrogen displacements from translational, rotational, and intramolecular motions, and comparing them to the actual displacements, it is found that one of the definitions fails, and the other performs reasonable well. It is found that the hydrogen displacements may very well be modeled by assuming independent translational and rotational motions. Attempts to obtain rotational diffusion coefficients from fitting the data using a symmetric diffusor model were unsuccessful. This was imputed to the large difference between the time scales for the different orientational motions and illustrates that experimental results should be met with reservation. © *1997 American Institute of Physics.* [S0021-9606(97)50519-8]

## I. INTRODUCTION

The large interest in crown ethers stems from their aptitude for selectively binding cations or small molecules. In this respect these substances are considered to be the simplest model systems containing enzyme specificity. In many of the theoretical[1] and experimental studies[2–6] the prototypical 18-crown-6 (1,4,7,10,13,16-hexaoxacylooctadecane) served as the object under investigation. It is one of the simplest macrocyclic systems, but sufficiently complex to cover the important characteristics of synthetic receptors, and is still of a computationally manageable size.

Theoretical calculations have demonstrated the high flexibility of 18-crown-6 and the existence of a multitude of low-energy conformations.[1] This flexibility is expected to be an important property in the role of 18-crown-6 as a catalyst.[7,8]

A large conformational freedom in solution and in the liquid state is suspected from the large experimental values of the electric dipole moments. In the apolar cyclohexane a value of 2.7 D was determined,[9] and in the pure liquid a molecular dipole moment as high as 3.3 D was found,[10] while the most important structures in the solid state are centrosymmetric.[11,12]

In previous papers we studied the dipole moment of 18-crown-6 in solution and in the liquid phase by means of molecular dynamics simulations.[13–15] Besides to the dipole moment, a great deal of attention was paid to the conformational statistics of the crown ether and the structure of the liquid. We also made extensive comparisons between a number of available potential models. It was found that in the liquid phase the simulated flexibility has a large effect on the static properties.[15]

In this paper we continue this project with the investigation of the dynamical behavior of 18-crown-6 in the liquid phase. Several papers were published concerning the experimental determination of transport properties of liquid 18-crown-6. Vogel and Weiss[16] studied by means of $^1$H-NMR spin-echo spectroscopy the self-diffusion of a number of nearly spherical and disklike molecules, among which was 18-crown-6, in the pure liquid phase. The dynamical behavior of 18-crown-6 was also studied using quasielastic neutron scattering by Lassegues *et al.*[17] who made an attempt to separate the dynamics into translational, rotational, and vibrational contributions. Richter and Zeidler[18] then again, examined self-diffusion and rotational diffusive motions by means of NMR relaxation experiments.

The models used in the above studies, for the interpretation of the experimental data are based on different approximations. To describe the reorientational motions of the molecules, Lassegues *et al.* used the approximation of spherical rotational diffusion. Richter and Zeidler, on the other hand, made use of an anisotropic diffusion model, thus taking into account the geometry of the molecules.

In this paper we use MD simulations to study the diffusive motions of 18-crown-6 in the liquid state at a single temperature. Three different potential models for the crown ether are employed. The aims of this investigation are twofold. First we want to investigate the possibility to separate the diffusive motions into different contributions. Translations can in principle always be decoupled from other motions, provided the MD run is long enough to ensure good statistics. As long as there is some separation of time scales it is attractive to describe the remaining motion of the molecule as a rotation, and a deformation. Because we are dealing with very flexible molecules it is of course not possible to completely separate both types of motion. Our aim is to find a definition of orientation, allowing for the best separa-

 0021-9606/97/106(19)/8140/9/$10.00 

tion possible, and by this elucidate the meaning of the experimentally obtained rotational diffusion coefficients.

The second aim is to examine if the potentials that are used, model a liquid that is comparable with the liquid used in experiments.

In the following section a theoretical framework is developed describing the rotations and deformations of the molecules. The computational details of the simulations are described in Sec. III. The results are discussed in Secs. IV and V, and Sec. VI presents our conclusions.

## II. ROTATIONS AND DEFORMATIONS OF THE INDIVIDUAL MOLECULES

In this section we shall refer all atomic position vectors with respect to the center-of-mass of the molecule, meaning that translations of the molecules have been dealt with already. Next, a working definition is needed to determine the orientation of the molecule, given the positions of all its constituting atoms. In the following we shall use several slightly different definitions. Here it is only important that we are giving for every configuration of the atoms, some set of three orthogonal unit vectors which we call the molecular reference frame.

We introduce the conditional probability density $P(\mathbf{r},\mathbf{r}_0;t)$ to find some atom $i$ near position $\mathbf{r}$ at time $t$, given that it occurred at position $\mathbf{r}_0$ at time $t=0$. We will now assume that we may write

$$P(\mathbf{r},\mathbf{r}_0;t)=G(\omega,\omega_0;t)g(\mathbf{x},\mathbf{x}_0;t). \tag{1}$$

Here $\omega$ and $\omega_0$ denote the orientation parameters of the molecular frame at time $t$ and at $t=0$; $\mathbf{x}$ and $\mathbf{x}_0$ are the position vectors of atom $i$ with respect to the molecular frame, again at time $t$ and $t=0$ respectively. Equation (1) says that the motion of the atom on average consists of two independent components, one resulting from the reorientation of the molecule, and one from the motion within the molecule. Of course, both types of motion will never be strictly independent, since the motion of all atoms together defines the changes of $\omega$. However, when the number of atoms per molecule is large enough, and the molecular frame is defined properly, Eq. (1) should be a reasonable approximation.

Our next step is to assume that the molecular reorientations may be described by a simple diffusion model of a symmetric diffusor. It has been shown by Favro[19] that the conditional probability or Green function $G(\omega,\omega_0;t)$ is the solution of

$$\frac{\partial}{\partial t}G(\omega,\omega_0;t)=-[D_1(P_a^2+P_b^2)+D_3P_c^2]G(\omega,\omega_0;t), \tag{2}$$

with initial value condition $G(\omega,\omega_0;0)=\delta(\omega-\omega_0)$. The constants $D_1$ and $D_3$ are the degenerate and unique eigenvalue of the diffusion tensor, which we assume to be parallel to the inertia tensor. $P_a$, $P_b$, and $P_c$ are the components of the angular momentum operator with respect to the molecular frame. Using[20,21]

$$\delta(\omega-\omega_0)=\frac{1}{8\pi^2}\sum_l (2l+1)\sum_{m,n} D_{m,n}^{(l)*}(\omega)D_{m,n}^{(l)}(\omega_0), \tag{3}$$

$$P^2D_{m,n}^{(l)}(\omega)=l(l+1)D_{m,n}^{(l)}(\omega), \tag{4}$$

$$P_cD_{m,n}^{(l)}(\omega)=mD_{m,n}^{(l)}(\omega), \tag{5}$$

with $P^2=P_a^2+P_b^2+P_c^2$, one easily derives[22–24]

$$G(\omega,\omega_0;t)=\frac{1}{8\pi^2}\sum_l (2l+1)e^{-l(l+1)D_1t}\times\sum_{m,n} D_{m,n}^{(l)*}(\omega)D_{m,n}^{(l)}(\omega_0)e^{-m^2(D_3-D_1)t}. \tag{6}$$

The Wigner functions $D_{m,n}^{(l)}(\omega)$ are defined with the convention of Edmonds.[20]

We are mainly interested to see how well the time scales of $G(\omega,\omega_0;t)$ and $g(\mathbf{x},\mathbf{x}_0;t)$ are separated. The rotational diffusion coefficients $D_1$ and $D_3$ can easily be obtained by calculating the time correlation functions of the axes of the molecular frame. An experimentalist would try to do this, for instance, by means of neutron scattering experiments, measuring the self-van Hove functions of the hydrogen atoms. We therefore set forth deriving expressions for these functions.

### A. Time correlation functions of molecular axes

Since the molecular axes do not diffuse within the molecular frame, we may forget about $g(\mathbf{x},\mathbf{x}_0;t)$ in Eq. (6). Denoting the molecular axes referred to the lab frame by $\hat{e}_\alpha$, and by $\hat{E}_\alpha$ when referred to the molecular frame, we may write

$$\langle\hat{e}_\alpha(t)\cdot\hat{e}_\alpha(0)\rangle=\int\frac{d\omega_0}{8\pi^2}\int d\omega\sum_m C_m^{(1)}[\hat{e}_\alpha(0)]\times C_m^{(1)*}[\hat{e}_\alpha(t)]G(\omega,\omega_0;t), \tag{7}$$

where $C_m^{(l)}(\hat{x})$ is a Racah spherical harmonic, and where we have used the spherical harmonic addition theorem.[20] Using[20,21]

$$C_m^{(l)}[\hat{e}_\alpha(t)]=\sum_n C_n^{(l)}(\hat{E}_\alpha)D_{n,m}^{(l)}[\omega(t)] \tag{8}$$

and the orthogonality of the Wigner functions, we obtain

$$\langle\hat{e}_\alpha(t)\cdot\hat{e}_\alpha(0)\rangle=e^{-2D_1t}\sum_m e^{-m^2(D_3-D_1)t}C_m^{(1)}(\hat{E}_\alpha)\times C_m^{(1)*}(\hat{E}_\alpha). \tag{9}$$

Applying this to the different axes we find

$$\langle\hat{e}_x(t)\cdot\hat{e}_x(0)\rangle=e^{-(D_1+D_3)t}, \tag{10}$$

$$\langle\hat{e}_y(t)\cdot\hat{e}_y(0)\rangle=e^{-(D_1+D_3)t}, \tag{11}$$

$$\langle\hat{e}_z(t)\cdot\hat{e}_z(0)\rangle=e^{-2D_1t}. \tag{12}$$

### B. Self-intermediate scattering function

The self-intermediate scattering function $F(k,t)$ is defined by

$$F(k,t)=\langle e^{i\mathbf{k}\cdot(\mathbf{r}(0)-\mathbf{r}(t))}\rangle, \tag{13}$$

where the brackets include an average over all atoms which contribute to the scattering, which in our case are the hydrogen atoms. Expansion of the exponent for small values of $k$ leads to

$$F(k,t)=1-\tfrac{1}{6}k^2\{\langle[x(t)-x(0)]^2\rangle+\langle[y(t)-y(0)]^2\rangle + \langle[z(t)-z(0)]^2\rangle\}. \tag{14}$$

Provided Eq. (1) is a valid approximation we can also write

$$F(k,t)=\int \frac{d\omega_0}{8\pi^2}\int d\omega\int d^3x_0\int d^3x\; e^{i\mathbf{k}\cdot(\mathbf{r}_0-\mathbf{r})} \times G(\omega,\omega_0;t)g(\mathbf{x},\mathbf{x}_0;t)\rho(\mathbf{x}_0), \tag{15}$$

where $\rho(\mathbf{x}_0)$ is the average distribution of hydrogen atoms in the molecule. Introducing

$$e^{i\mathbf{k}\cdot\mathbf{r}}=\sum_l\sum_m (i)^l(2l+1)j_l(kr)C_m^{(l)*}(\hat{r})C_m^{(l)}(\hat{k}), \tag{16}$$

and using the analog of Eq. (8) for $C_m^{(l)}(\hat{r})$, the orthogonality of the Wigner functions, and

$$\sum_m C_m^{(l)}(\hat{k})C_m^{(l)*}(\hat{k})=1, \tag{17}$$

one finds after some tedious algebra

$$F(k,t)=\sum_l (2l+1)e^{-l(l+1)D_1t}\sum_m e^{-m^2(D_3-D_1)t} \times\int d^3x_0\int d^3x\; j_l(kx_0)j_l(kx)C_m^{(l)*}(\hat{x}_0)C_m^{(l)} \times(\hat{x})g(\mathbf{x},\mathbf{x}_0;t)\rho(\mathbf{x}_0). \tag{18}$$

### C. Self-intermediate scattering function at small values of *k*

We shall now analyze Eq. (18) at small values of $k$. Using

$$j_0(z)=\frac{\sin z}{z}\approx 1-\frac{1}{6}z^2+\frac{1}{120}z^4-\cdots, \tag{19}$$

$$j_1(z)=\frac{1}{z}\left(\frac{\sin z}{z}-\cos z\right)\approx\frac{1}{3}z-\frac{1}{30}z^3+\cdots, \tag{20}$$

and defining

$$\Psi(t)=\lim_{k\to 0}\frac{1-F(k,t)}{k^2}, \tag{21}$$

we obtain

$$\Psi(t)=\tfrac{1}{6}\int d^3x_0\int d^3x(x_0^2+x^2)g(\mathbf{x},\mathbf{x}_0;t)\rho(\mathbf{x}_0) - \tfrac{1}{3}e^{-2D_1t}\sum_m e^{-m^2(D_3-D_1)t}\int d^3x_0\int d^3x\; x_0x \times C_m^{(1)*}(\hat{x}_0)C_m^{(1)}(\hat{x})g(\mathbf{x},\mathbf{x}_0;t)\rho(\mathbf{x}_0). \tag{22}$$

Writing out this expression results in

$$\Psi(t)=A_0-\tfrac{1}{3}\langle z(t)z(0)\rangle e^{-2D_1t}-\tfrac{1}{3}\{\langle x(t)x(0)\rangle + \langle y(t)y(0)\rangle\}e^{-(D_1+D_3)t}, \tag{23}$$

where the time correlation functions should be calculated in the molecular reference frame. The precise definition of the geometric factor $A_0$ is given below [Eq. (26)].

In order to make further progress we now assume specific models for $\rho(\mathbf{x}_0)$ and $g(\mathbf{x},\mathbf{x}_0;t)$. Of course $\rho(\mathbf{x}_0)$ may be easily obtained from the simulation data, but it will be much more difficult to develop a model for $g(\mathbf{x},\mathbf{x}_0;t)$. Since we are mainly interested to investigate the possibility of separation of time scales, we shall restrict our attention to two extremes. First, when the motion within the molecule is fast and over small distances only, $\Psi(t)$ will quickly rise at short times, and next, at longer times, be governed by the rotational diffusive motion over much larger distances. In Eq. (22) we may forget about $g(\mathbf{x},\mathbf{x}_0;t)$ at these values of $t$, and put $\mathbf{x}\approx\mathbf{x}_0$. Secondly, when the motion within the molecule is substantial, but much slower than the rotational diffusion we may replace $g(\mathbf{x},\mathbf{x}_0;t)$ with its initial value $\delta(\mathbf{x}-\mathbf{x}_0)$, which after integration over $\mathbf{x}$ also leads to $\mathbf{x}\approx\mathbf{x}_0$.

We now expand the density in the form

$$\rho(\mathbf{x})=\sum_l\sum_m \rho_{l,6m}(x)C_{6m}^{(l)}(\hat{x}), \tag{24}$$

where the index $6m$ in the above equation represents the sixfold symmetry displayed by the average distribution of the hydrogen atoms (see Fig. 1).

If $\Psi(t)$ is calculated using the above approximation concerning $g(\mathbf{x},\mathbf{x}_0;t)$, we obtain

$$\Psi(t)=A_0\{1-\tfrac{1}{3}(1+\tfrac{2}{5}B_2)e^{-2D_1t} - \tfrac{2}{3}(1-\tfrac{1}{5}B_2)e^{-(D_1+D_3)t}\} \tag{25}$$

with

$$A_0=\tfrac{4}{3}\pi\int dx\; x^4\rho_0(x)=\tfrac{1}{3}\int d^3x\; x^2\rho(\mathbf{x}), \tag{26}$$

$$A_2=\tfrac{4}{3}\pi\int dx\; x^4\rho_2(x)=\tfrac{5}{3}\int d^3x\; x^2P_2(\cos\theta)\rho(\mathbf{x}), \tag{27}$$

$$B_2=A_2/A_0. \tag{28}$$

Two interesting things may be noted. First, when $D_1=D_3$, terms with $B_2$ cancel. Secondly, it may happen that the scattering mass is distributed spherically, in which case $B_2=0$,

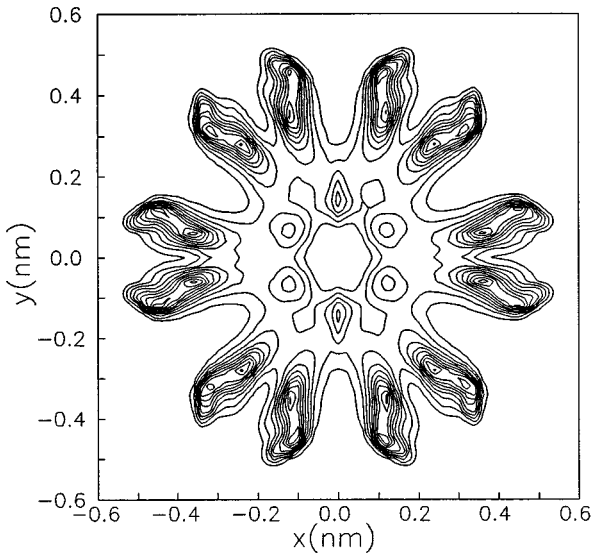


FIG. 1. Contourplot of the average distribution of the hydrogen atoms from the simulation with potential **C**. The positions of the atoms are projected on the plane formed by the $x$ and $y$ axis obtained with the rotation matrix.

while at the same time $D_1 \neq D_3$. In this latter case $\Psi(t)$ still has contributions from two different exponential terms.

## III. METHODS

A total of three simulations was performed using three different potential models, referred to as potentials **A**, **B**, and **C**.

Potential **A** combines parameters from the AMBER all-atom force field[25] with charges determined by Szentpály and Shamovsky.[26] These charges resulted from a fitting procedure in which the empirical force field energies of seven conformers of the crown were fitted to their *ab initio* energies. The *ab initio* calculations included electron correlation via full second order Møller–Plesset perturbation theory, employing the 6-31 G basis set. This set of charges is expected to include effects of intramolecular polarization.

Potentials **B** and **C** both use the united atom approach. Potential **B** combines the GROMOS united atom force field[27] with a Fourier series for the torsion potential, emerging from fitting the MM2 result to the conformational space of 1,2-dimethoxyethane, without the use of nonbonded 1–4 terms.[28] The charges were taken from the electrostatic potential calculations of Singh and Kollman.[29] These calculations, for which small fragments of the crown ether were used, were done on the Hartree–Fock/6-31 G* level. Apart from slightly different charges, this potential was used by Kowall and Geiger in their study of the structure and dynamics of the hydration shell of 18-crown-6 and their calculation of the free energy for association of 18-crown-6 and $K^+$ in water.[30,31]

Potential **C** differs from **B** in only the torsional part of the potential. In this case all parameters were taken from the GROMOS force field. The charges were the same as for **B**.

A modified version of the GROMOS simulation package[27] was used. Electrostatic interactions were evaluated with the Ewald summation technique. 125 molecules were confined in a cubic box and the systems were held a constant temperature of 343 K and at a pressure of 1 atm. All bonds were kept at their equilibrium lengths using the SHAKE algorithm.[32] The MD simulation with potential model **A** was run for a total of 500 ps; those with models **B** and **C** both for 1000 ps. Further details concerning these simulations can be found in Ref. 15.

In order to be able to study reorientation processes of the molecules, a molecule-fixed frame of axes is needed. Two different types of reference frames were determined. The first type is formed by the eigenvectors of the inertia tensor. In Ref. 13 we have seen that on average the molecular shape resembles that of a flattened ellipsoid. The eigenvector belonging to the largest eigenvalue was found to be roughly normal to the plane which minimizes the sum of the squared distances of all atoms to that plane, and will be called the $z$ axis.

As a result of the molecule's conformational freedom, the eigenvalues of the two inplane axes can become (nearly) degenerate, in which case they are not uniquely defined. In order to make the $x$ and $y$ axes move as smoothly as possible, we diagonalized the inertia tensor in the frame of the previous sample. As a result, these axes are not ordered according to the corresponding eigenvalues; in fact both axes are equivalent.

The second type of molecular frame that we used, was obtained by rotating some reference molecule and its molecular frame, such that in a second step the actual molecule could be obtained by simply deforming the rotated reference molecule along its rotated normal modes. The reference structure was chosen to be the highly symmetrical $D_{3d}$ conformation positioned in the $xy$ plane. The origin of the reference frame coincided with the center-of-mass of the molecule. Also with this definition, the two in-plane axes are equivalent. Details of the algorithm used to calculate these parameters will be given elsewhere.[33]

The rotation matrix method as we have used it has the disadvantage that the orientations of the molecules are determined with respect to one single reference structure. One might prefer to determine the rotation relative to the previous form sampled. Then, the ultimate rotation matrix at a certain time, is the product of a series of matrices, each of which describes the rotation between two successive samples. Unfortunately, this procedure leads to many difficult numerical problems. Moreover, also in this case Eq. (1) would not be guaranteed. Therefore, we restrict ourselves to the two definitions given above.

## IV. TIME CORRELATION FUNCTIONS

### A. Translational motion

The self-diffusion constants $D_T$ were determined from the mean-square displacement of the center-of-masses according to the Einstein equation:

$$D_T = \lim_{t\to\infty} \frac{1}{6t} \langle [\mathbf{r}(t) - \mathbf{r}(0)]^2 \rangle. \tag{29}$$

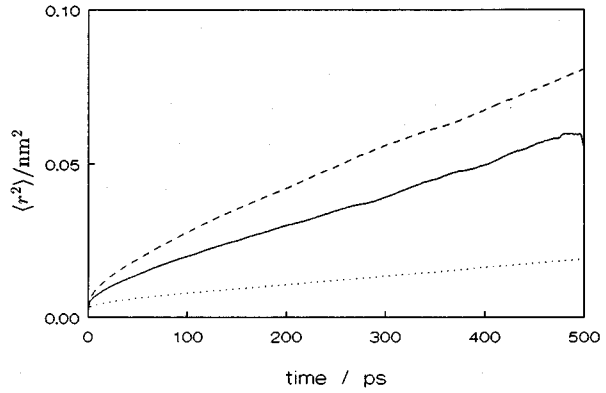


FIG. 2. Mean-square displacements of the center-of-masses. The solid line correspond with potential **A** (no Ewald sums used). The dotted line corresponds with potential **B**, and the dashed line with potential **C**.

The mean-square displacements (m.s.d.) as a function of time are displayed in Fig. 2. The m.s.d. from the simulation with potential **A**, using the Ewald technique, at $\sim 325$ ps showed a change in the slope which could not be attributed to any kind of drift of the system as a whole, nor to systematic fluctuations in the dimensions of the computational box. Because it is doubtful that this change in the slope has any physical meaning this simulation will not be regarded in the remainder of this paper. We therefore performed a new simulation with the same potential **A**, keeping all parameters etc. the same, but without using Ewald sums; electrostatic interactions were neglected beyond the cutoff radius. The system was newly initialized and equilibrated as described in Ref. 15. The m.s.d. of the center-of-masses obtained from this run is represented by the solid curve in Fig. 2. This time no change in the slope is observed.

With potentials **B** and **C** no problems were met using the Ewald method. The self-diffusion coefficients determined from Fig. 2, together with experimental results are given in Table I. The diffusion coefficient with potential **B** is found to be much too low. Potential **A**, and especially potential **C**, compare rather well with experiment.

### B. Rotations of molecule-fixed reference frames

In Sec. III we defined two types of molecular frames of axes. In the theoretical section it was shown that rotational diffusion coefficients may be obtained from correlation functions of the individual axes [Eqs. (10)–(12)]. In Fig. 3 these correlation functions are displayed for the three potential models and for both types of reference frames.

The two in-plane axes are indeed equivalent, but their

TABLE I. Self-diffusion coefficients[a] calculated from mean-square displacements (see Fig. 2).

| | Simulations | | |
|---|---|---|---|
| Potential model | With Ewald | Without Ewald | Experiment |
| **A** | ⋯ | 1.05 | 1.45[b]/2.1[c]/1.81[d] |
| **B** | 0.28 | ⋯ | |
| **C** | 1.41 | ⋯ | |

[a]Values times $10^6$ cm$^2$/s.
[b]From Ref. 16.
[c]From Ref. 17. $T=353$ K.
[d]From Ref. 18. Value extrapolated for $T=343$ K.

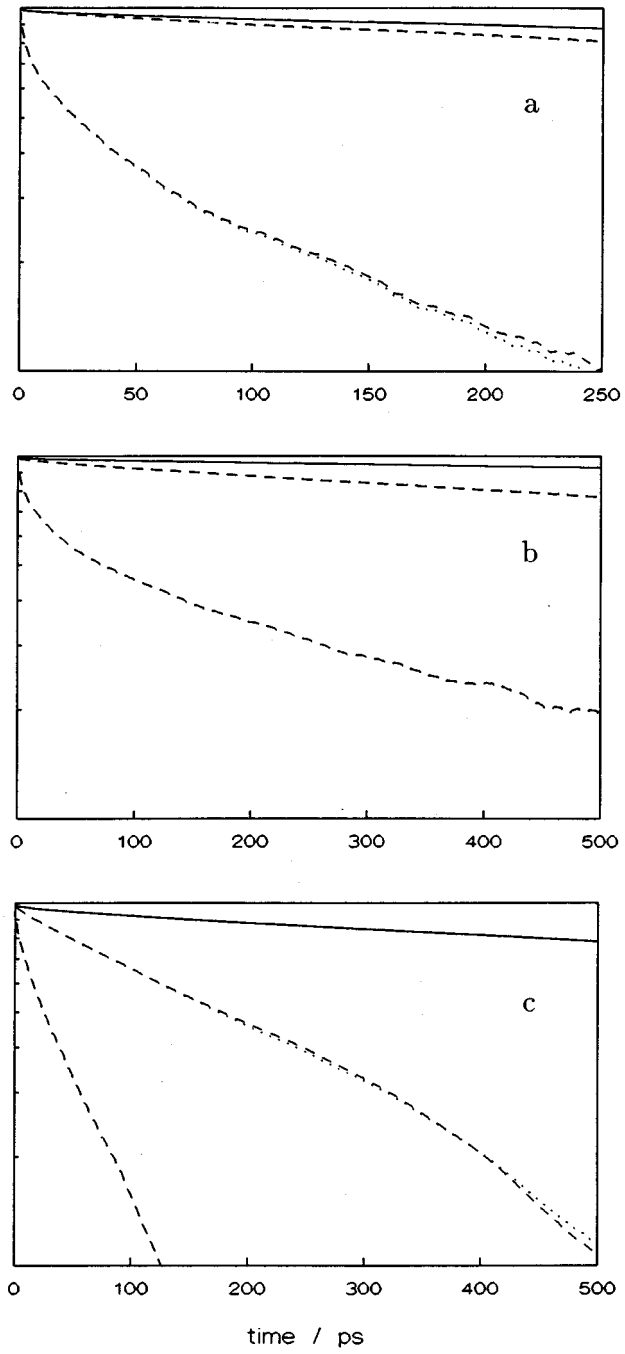


FIG. 3. (a) Normalized time-autocorrelation functions of the axes of the molecular reference frame. Results for potential **A** (without Ewald method). The solid line represents the correlation function of the $z$ axes (the functions for the inertia tensor and the rotation matrix can not be distinguished). The two lines in the middle correspond with the $x$ and $y$ axes from the rotation matrix. The lower lines (not distinguishable) belong the $x$ and $y$ axes from the inertia tensor. (b) For potential **B**. (c) For potential **C** ($y$ axes are on log scale).

TABLE II. Rotational diffusion coefficients[a] determined from time correlation functions.

| Potential model | Diffusion coefficient | Type frame of axes: Inertia tensor | Type frame of axes: Rotation matrix | Experiment[c] |
|---|---|---|---|---|
| **A**[b] | $D_1$ | 0.19 | 0.19 | 2.04 |
| | $D_3$ | 5.92 | 0.56 | 24.10 |
| **B** | $D_1$ | 0.05 | 0.05 | 2.04 |
| | $D_3$ | 1.73 | 0.40 | 24.10 |
| **C** | $D_1$ | 0.20 | 0.20 | 2.04 |
| | $D_3$ | 18.73 | 4.65 | 24.10 |

[a]Values times $10^{-9}$ $s^{-1}$.
[b]Simulation with this potential model was without the Ewald sum method.
[c]From Ref. 18. Values extrapolated for $T=343$ K.

behavior depends very much on the way they are defined. The correlation functions for the $z$ axes emerging from both methods are found to be virtually identical. The rotational diffusion coefficients determined from these correlation functions are collected in Table II.

The coefficients found for **A** are in between of those for potentials **B** and **C** where the Ewald method was used for the treatment of the long-range forces. The diffusion coefficients with potential **B** are again smaller than those obtained with the other potentials. Although the molecules are rather flexible in this case (see Ref. 15), the correlation functions decorrelate much slower, especially at large times. Apparently, the molecules easily adjust to every fluctuation in their environment, without appreciably changing their orientations; this results in a fast decay only at small values of $t$. The relatively low barriers to dihedral transitions, not only influence the static, but also the dynamic properties. This may also explain the peculiar behavior of the total dipole fluctuation densities observed in Ref. 15. Because the molecular dipole moment was found to be correlated with the $z$ axis, the long correlation times will cause long-time fluctuations in the total dipole moment fluctuation densities [see Fig. 1(b) of Ref. 15].

Potential **C** differs from potential **B** only by its flexibility, modeling molecules that are more rigid.[15] Potential **C** molecules do not have the possibility to adjust so easily to every fluctuation as do potential **B** molecules, and are therefore much more persistent in their reorientational motions. This results in much larger longe time diffusion coefficients. On the basis of a comparison with experiment it seems that the inertia tensor method performs somewhat better (Table II).

In order to investigate the difference in behavior of the two types of molecular axes, we have plotted in Fig. 4, for one of the molecules, the paths of the $z$ component of the three eigenvectors of the inertia tensor (the other components were found to behave similarly and are not shown). In Fig. 5 the corresponding paths obtained with the rotation matrix are given. It is clear that the orientations of the $x$ and $y$ axes with the first definition are rather sensitive to conformational changes. They consequently fluctuate wildly, resulting in the fast decorrelation seen in Fig. 3. It is also clear that the

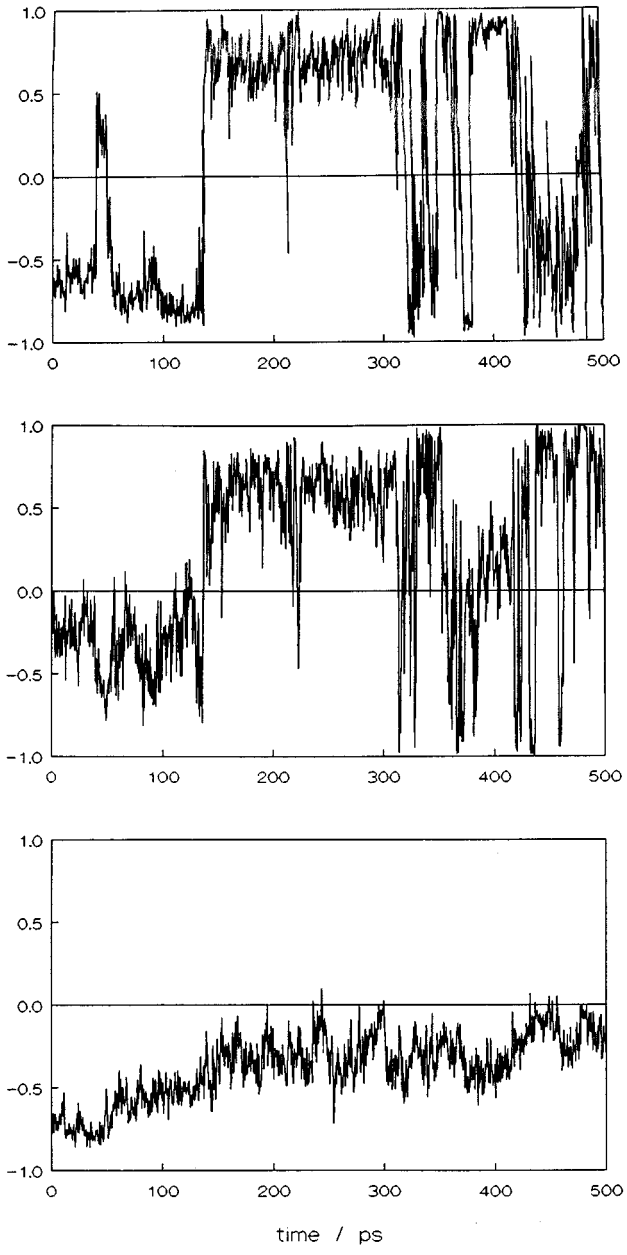


FIG. 4. $z$ components of axes of the molecular reference frame as a function of time for one of the molecules with potential **C**. $z$ component of the $x$ axis (top); of the $y$ axis (middle); and of the $z$ axis (bottom). Reference frame obtained from the inertia tensor.

method of the inertia tensor remains liable to fluctuations caused by the degeneracy problem mentioned in Sec. III, which will also contribute to the decay of the correlation functions. The orientation of the $z$ axis is less influenced by deformations of the molecules and displays a more pure diffusion behavior. Figure 5 demonstrates that when the axes are obtained with the rotation matrix, they all show more or less real diffusion behavior. The $z$ axis in this case is virtually identical to that of Fig. 4.

## V. SCATTERING FUNCTIONS

In this section we restrict ourselves to results obtained with potential **C**. The reason is that the translational and

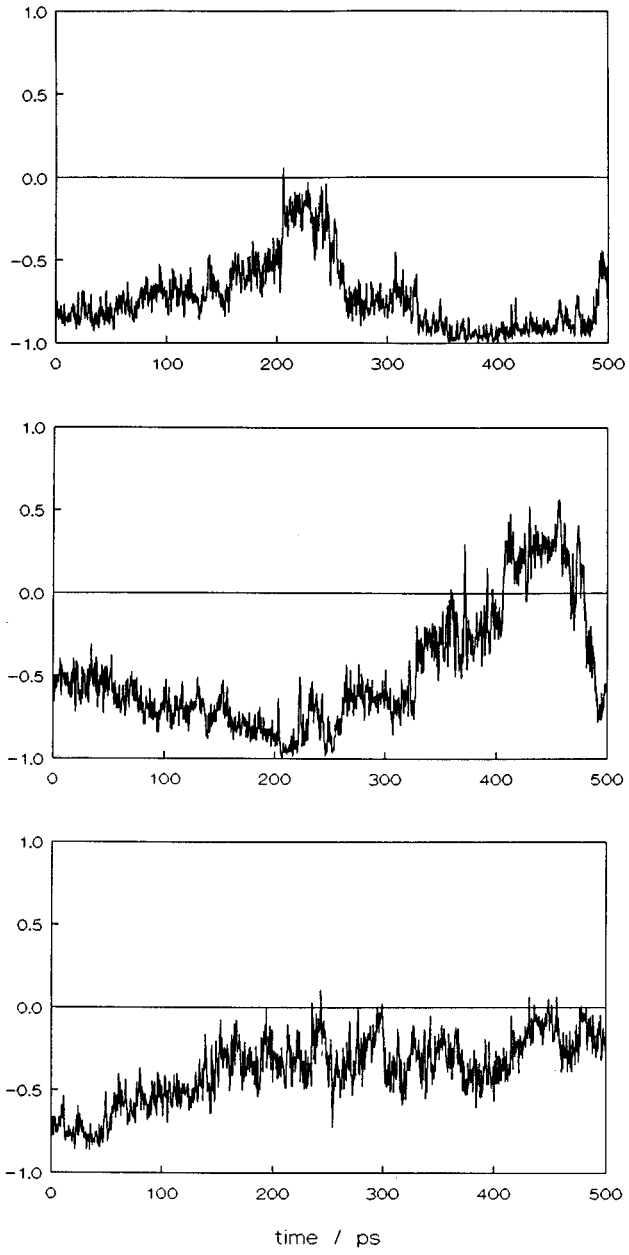


FIG. 5. As Fig. 4, but now for the reference frame from the rotation matrix.

rotational diffusion coefficients obtained with this potential model compare best with experimental values (see Tables I and II). Because the hydrogen atoms were not simulated explicitly, their positions had to be calculated first.

### A. Separation of translational and remaining motions

Due to the strong spin-dependence of the neutron–proton interaction, hydrogen has an incoherent cross section which is extraordinary large compared to its coherent cross section; it is also large compared to the scattering cross sections of practically all other elements. Therefore, scattering on a hydrogen rich compound like 18-crown-6, to a good approximation, is described by the incoherent scattering functions. With time resolved experiments the incoherent intermediate scattering function Eq. (13) is measured, given by the space Fourier transform of the self-van Hove function $G_s(\mathbf{r},t)$,

$$G_s(\mathbf{r},t)=N^{-1}\left\langle \sum_{i=1}^{N} \delta\{\mathbf{r}-[\mathbf{r}_i(t)-\mathbf{r}_i(0)]\}\right\rangle, \tag{30}$$

where the vectors $\mathbf{r}_i$ are the position vectors of the hydrogen atoms.

In case the displacement of the scatterers result from two independent types of motion, the intermediate scattering function is the product of two factors, one for each type of motion. Here we investigate the independence of the translations of the center-of-masses of the molecules and the remaining contributions to the hydrogen displacements. The intermediate scattering function should be the product of a translational factor $F^T(k,t)$ and a factor $F^{R,D}(k,t)$ resulting from the displacements with respect to the center-of-masses

$$F(k,t)=F^T(k,t)F^{R,D}(k,t). \tag{31}$$

We have checked this relation, and have found that it holds true to a very good degree, meaning that in our box, molecular translations are indeed decoupled from other types of motion.

If the translational displacements obey Gaussian statistics, the corresponding intermediate scattering function reads

$$F^T(k,t)=\exp(-D_T k^2 t). \tag{32}$$

We have found that with our box, this relation holds true over the entire range of $k$ and $t$ values. A similar check is offered by

$$\langle r^2(t)\rangle=\int r^2 G_s(\mathbf{r},t)d\mathbf{r}=6Dt, \tag{33}$$

which was also found to hold true.

### B. Separation of internal and rotational motions

In Sec. II C the self-intermediate scattering function $F^{R,D}(k,t)$ was analyzed at small values of $k$. Two different formulas were presented, both of them assuming that rotations and deformations may be treated as independent types of motion. The first expression, Eq. (23), assumes that the motion within the molecule is substantial, and must be calculated directly from the MD data. The second, Eq. (25), assumes that the motion within the molecule may be neglected altogether, either because it is too fast to be seen at long times, or it is too slow to be seen at all times covered in the present study. We shall investigate both expressions, using the two definitions of molecular frames given in Sec. III.

We first concentrate on Eq. (25). In the case of spherical rotational diffusion, i.e., when $D_1=D_3$, Eq. (25) reads

$$\Psi(t)=A_0(1-e^{-2Dt}). \tag{34}$$

We have fitted this expression to the exact values of $\Psi(t)$, obtained from Eqs. (14) and (21), considering the rotational diffusion coefficient, $D$, and $A_0=\frac{1}{3}\langle r^2\rangle$ as independent parameters. The fit was restricted to values of $t$ in the range from 250 to 1000 ps, since the influence of dihedral transi-

TABLE III. Rotational diffusion coefficients and geometric parameters occurring in Eq. (25).

| Parameter | Calculated from first principles | | |
|---|---|---|---|
| | I[a] | II[b] | III[c] |
| $D_1$[d] | 0.20 | 0.20 | 0.20 |
| $D_3$[d] | 18.73 | 11.42 | 4.65 |
| $A_0$[e] | 0.0509 | 0.0509 | 0.0509 |
| $B_2$ | −1.9477 | −1.9582 | −1.9477 |

[a]Inertia tensor calculated from all atoms.
[b]Inertia tensor calculated from only hydrogen atoms.
[c]Rotation matrix.
[d]Values times $10^{-9}$ $s^{-1}$.
[e]In $nm^2$.

tions is expected to be most important at small values of $t$.[17] Values of 3.89 Å and $2.2\times10^9$ $s^{-1}$ were found for the root mean-square radius $r$ of the molecules, and for $D$, respectively. The value of $r$ compares very well with the value of 3.91 Å calculated directly from the simulation data. The result for the rotational diffusion coefficient is in excellent agreement with the experimental value of $2.3\pm0.8\times10^9$ $s^{-1}$ reported by Lassegues *et al.* From these results we conclude that the liquid modeled with potential **C** rather well resembles the experimental liquid. A fit over the entire range of $t$ values results in a smaller particle diameter (by 1%) and a larger rotational diffusion coefficient (by 8%).

Using the values for $D_r$, and $r$ calculated above one can calculate the viscosity from the Stokes–Einstein formula

$$D_r=\frac{k_BT}{8\pi\eta r^3 f_r}, \tag{35}$$

with the additional correction factor $f_r$. For neat liquids, $f_r$ is assumed to have a value of 1/6.[34] For $\eta$ a value of 8.730 mPa s is found ($T=343$ K). This is somewhat larger than the 6.721 mPa s determined by Vogel and Weiss.[16]

We now continue to investigate the merits of Eq. (25) in the case of a symmetric diffusor. In attempting to fit this function to the calculated $\Psi(t)$, considering $A_0$, $B_2$, $D_1$, and $D_3$ as the independent parameters, it was found that the results from the fit were very sensitive for the initial values of these parameters. For instance, equally good fits were found while $B_2$ having different signs. As a test we performed a fitting procedure of $\Psi(t)$ that was constructed from parameters obtained from first principles. Also in this case it was found that totally different sets of parameters gave fits of the same quality. Neglecting the first 200 ps of the function or taking the entire range from 0 to 1000 ps made no significant difference. Apparently, it does not seem possible to fit two phenomena that take place on such different time scales with one function.

In Table III we give the values of all parameters obtained from first principles. Also included in this table are the results obtained with molecular frames defined slightly different from those obtained with the inertia tensor. Since only hydrogen atoms contribute to $F(k,t)$, and hence $\Psi(t)$, one may choose to restrict attention to the hydrogen atoms also when calculating the inertia tensor. This amounts to considering the motion of the other atoms in the molecule as contributing to the thermal bath. Considering only the hydrogen atoms has a substantial effect only on $D_3$.

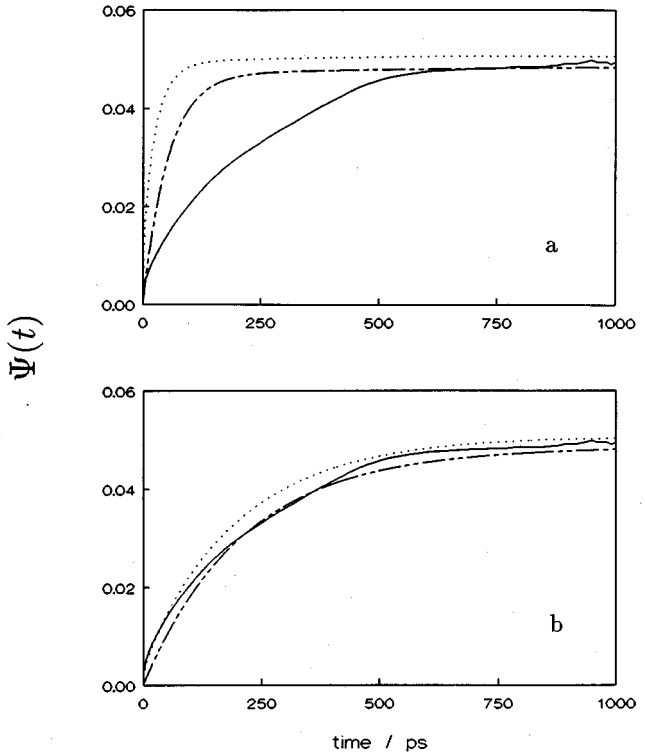


FIG. 6. (a) The scattering function $F(k,t)$ for $k\to0$ [solid line; see Eq. (14)]. The dash–dotted line and the dotted line represent $\Psi(t)$ calculated from first principles, respectively, for the model neglecting intramolecular motions [Eq. (25)], and the model including intramolecular motions [Eq. (23)]. For the calculated $\Psi(t)$'s, the values of $D_1$ and $D_3$ from the inertia tensor were used. (b) As in (a), but now $D_1$ and $D_3$ from the rotation matrix were used for the calculation of $\Psi(t)$ from first principles.

In Fig. 6 we have plotted $\Psi(t)$ calculated according to Eqs. (11) and (14) (solid lines), together with $\Psi(t)$ obtained from Eq. (25) using the parameters $A_0$, $B_2$, $D_1$, and $D_3$ from first principles (dash–dotted lines). The result obtained with the use of the inertia tensor, Fig. 6(a), is seen to rise much faster than the exact $\Psi(t)$. The most obvious explanation is that this method considerably overestimates the speed of the reorientational motions. Above it was illustrated that with this method it is hard to discriminate between deformations and rotational motions (see Fig. 4). This means that the value for $D_3$ is probably estimated too large although this coefficient compares rather well with experiment (see Table II). In connection with the above discussion about the difficulties with the fitting procedure, one should be sceptic with respect to the experimental results.

Using molecular frames by use of the rotation matrix gives results that compare reasonably well with the exact values of $\Psi(t)$ [Fig. 6(b)]. At small values of $t$, however, it seriously underestimates $\Psi(t)$. Apparently, this procedure takes into account only rather small contributions from the deformations.

Finally, we concentrate on the results obtained with Eq.

(23) (dotted lines in Fig. 6). The correlation functions occurring in this equation were calculated using hydrogen coordinates with respect to the molecular reference frames. This time, in both cases $\Psi(t)$ rises much faster than in the above cases. This result is rather obvious since Eq. (23) can only overestimate the motions of the atoms. At small values of $t$, however, as long as displacements are rather small, the rotation matrix method should provide a reasonable separation of rotations and deformations. Indeed, it is seen in Fig. 6(b) that with this method the exact $\Psi(t)$ is reproduced almost exactly for times up to 55 ps.

The calculations of this section clearly demonstrate that reorientations and dihedral transitions take place on comparable time scales.

## VI. CONCLUSIONS

We have investigated diffusive motions of 18-crown-6 in the liquid phase by means of molecular dynamics simulations. Three different force fields for the crown ether were tested. In two of the three simulations the long-range Coulombic interactions were handled with the Ewald method.

Translational diffusion coefficients were determined from the mean-square displacement of the center-of-masses of the molecules. The three potential models perform quite differently. The diffusion coefficient obtained with potential **A** is in reasonable agreement with experimental data, while the one obtained with potential **C** even compares fairly well. Potential **B** is too flexible and its diffusion coefficient is much too small.

Rotational diffusion was studied with potential **C**, using a model for spherical diffusors. The results were in good agreement with those of neutron scattering experiments by Lassegues *et al.*

When looking at computed displacements of the hydrogen atoms with respect to the center-of-masses of the molecules, it is possible to discern two different time regimes. It is tempting to relate them to the two diffusive motions of a symmetric diffusor. To give a meaning to the diffusion coefficients, one needs a definition of the rotating molecular frame, that allows for the best separation of rotational and intramolecular motions possible.

We have investigated two different definitions of molecular frames. With the first, the principal axes of inertia are taken to constitute the molecular frame. By calculating the molecular diffusion, and combining this with the intramolecular motions, we found that this definition fails badly.

With the second definition, a $D_{3d}$ reference molecule is rotated such that in a second step the actual molecule may be obtained by deformation along the normal coordinates of the rotated molecule. Hydrogen displacement obtained by combining rotational and intramolecular motions, were in reasonable agreement with the actual displacements, obtained directly from the MD data. Attempts to extract the diffusion coefficients from fitting the data using a symmetric diffusor model were unsuccessful. The time regimes for both reorientational processes differ too much to be treated in one fit.

In general, experimental results contain a certain degree of inaccuracy. If the error bars are substantial such as to enclose all curves depicted in Fig. 6(b), it is clear that fitting the experimental data may yield a wide spectrum of diffusion coefficients. Reported diffusion coefficients should therefore be met with reservation.

## ACKNOWLEDGMENTS

The authors want to thank W. K. den Otter and N. F. A. van der Vegt for their computational assistance.

[1] R. B. Shirts and L. D. Stolworthy, J. Inclus. Phenom. **20**, 297 (1995), and references therein.
[2] J. Dale and P. O. Kristiansen, Acta Chem. Scand. **26**, 1471 (1972).
[3] C. I. Ratcliffe, J. A. Ripmeester, G. W. Buchanan, and J. K. Denike, J. Am. Chem. Soc. **114**, 3294 (1992).
[4] K. Fukuhara, K. Ikeda, and H. Matsuura, Spectrochim. Acta A Mol. Spectrosc. **50**, 1619 (1994).
[5] J. T. Chuang and J. G. Lo, J. Radioanal. Nucl. Chem. **189**, 307 (1995).
[6] M. Pimpl, J. Radioanal. Nucl. Chem. **194**, 311 (1995).
[7] J. M. Lehn, Acc. Chem. Res. **11**, 49 (1978).
[8] J. C. Hogan and R. D. Gandour, J. Am. Chem. Soc. **102**, 2865 (1980).
[9] R. Caswell and D. S. Suvannunt, J. Heterocyclic Chem. **25**, 73 (1988).
[10] R. Perrin, C. Decoret, G. Bertholon, and R. Lamartine, Nouv. J. Chim. **7**, 263 (1983).
[11] M. Dobler, Chimia **38**, 415 (1980).
[12] T. M. Fyles and R. D. Gandour, J. Inclus. Phenom. **12**, 313 (1992).
[13] F. T. H. Leuwerink and W. J. Briels, J. Chem. Phys. **103**, 4637 (1995).
[14] F. T. H. Leuwerink and W. J. Briels, J. Phys. Chem. **99**, 16549 (1995).
[15] F. T. H. Leuwerink and W. J. Briels, J. Phys. Chem. B **101**, 1024 (1997).
[16] H. Vogel and A. Weiss, Ber. Bunsenges. Phys. Chem. **85**, 539 (1981).
[17] J. C. Lassegues, M. Fouassier, and J. L. Viovy, Mol. Phys. **50**, 417 (1983).
[18] H. Richter and M. D. Zeidler, Mol. Phys. **55**, 49 (1985).
[19] D. L. Favro, Phys. Rev. **119**, 53 (1960).
[20] A. R. Edmonds, *Angular Momentum in Quantum Mechanics* (Princeton University Press, Princeton, NJ, 1960).
[21] W. J. Briels, J. Chem. Phys. **73**, 1850 (1980).
[22] D. L. Favro, *Rotational Brownian Motion in: Fluctuation Phenomena in Solids*, edited by R. E. Burgess (Academic, New York, 1965).
[23] B. J. Berne and R. Pecora, *Dynamical Light Scattering* (Wiley, New York, 1976).
[24] H. Versmold, Z. Naturforsch. Teil A **25**, 367 (1970).
[25] S. J. Weiner, P. A. Kollman, D. T. Nguyen, and D. A. Case, J. Comput. Chem. **7**, 230 (1986).
[26] L. von Szentpály and I. L. Shamovsky, J. Mol. Struct. (Theochem) **305**, 249 (1994).
[27] W. F. van Gunsteren and H. J. C. Berendsen, Groningen Molecular Simulation Library. Groningen, The Netherlands, 1987.
[28] D. Bressanini, A. Gamba, and G. Morosi, J. Phys. Chem. **94**, 4299 (1990).
[29] U. C. Singh and P. A. Kollman, J. Comput. Chem. **5**, 129 (1984).
[30] T. Kowall and A. Geiger, J. Phys. Chem. **98**, 6216 (1994).
[31] T. Kowall and A. Geiger, J. Phys. Chem. **99**, 5240 (1995).
[32] J. Ryckaert, G. Ciccoti, and H. J. C. Berendsen, J. Comput. Phys. **23**, 327 (1977).
[33] W. K. den Otter and W. J. Briels, J. Chem. Phys. **106**, 5494 (1997).
[34] J. T. Hynes, R. Kapral, and M. Weinberg, J. Chem. Phys. **69**, 2725 (1978).